1.8 Absolute Quantum Efficiency of ACIS Flight Detectors

1.8.1 Quantum Efficiency Model and Fitting Results

In this section we present the best-estimate absolute quantum efficiency, as of this writing, for each flight device. In each case the absolute quantum efficiency has been derived from measurements of the relative quantum efficiency of the flight devices, with respect to reference detectors, described above in section 1.7.2, together with the absolute quantum efficiency models of the reference detectors described in section 1.6.1.

We are confident that we understand the accuracy of quantum efficiency models for the front-illuminated (FI) detectors, and we discuss this subject at some length here. On the other hand, the models we present for back-illuminated (BI) devices are not particularly accurate, and, perhaps worse, the errors in the back-illuminated models are not well characterized. Thus the BI models given here must be regarded as interim products. Fortunately, we have very recently identified the origin of at least a large fraction of the fairly large, (i.e. 10-20%) systematic errors in our current analysis of BI CCD data. In short, we now believe it is essential to use accurate models of both source spectrum and detector spectral redistribution to obtain reliable quantum efficiency measurements for these devices. This more accurate analysis has not been completed at this writing, but we are confident that it can be done. See section 1.7.3 for a brief quantitative discussion of these errors.

We have used the so-called "slab and stop" model of the ACIS CCD gate structure, described in section 1.1, to model detector quantum efficiencies. For clarity, the various slab-and-stop model parameters used in the model of FI detector quantum efficiency are re-presented in Table 1.62. Note that only four model parameters were varied in fits to measurements made with the flight detectors. The remaining three parameters were constrained by mesh measurements (see section 1.5) or by scanning electron micrograph (SEM) measurements of siblings of the flight devices.

1.8.2 Fitting Methods: FI Device Model Parameters.

The spatially-averaged relative quantum efficiency measurements described in section 1.7.2 were used to constrain slab-and-stop model gate structure parameters for the flight FI devices. For each device, the MIT CSR relative efficiency measurements at 525 eV, 677 eV, 1740 eV and 2015 eV were used to fit for three model parameters: the mean silicon gate thickness, the mean silicon dioxide thickness, and the silicon nitride thickness. In each case, the reference detector quantum efficiency was modelled using the slab and stop model parameters derived from the undispersed synchrotron measurements, as described

Parameter	Determined from:	See Section:
Poly-silicon gate thickness	Fit to flight-device relative QE data	1.7.2
SiO_2 insulator thickness	Fit to flight-device relative QE data	1.7.2
Si_3N_4 insulator thickness	Fit to flight-device relative QE data	1.7.2
Depletion depth	Fit to flight-device branching ratio data at 5.9 keV	1.6.2
Channel Stop width	Mesh and SEM measurements‡ on sibling devices	1.5
Channel Stop SiO_2 thickness	Mesh and SEM measurements on sibling devices	1.5
Channel Stop Si P^+ thickness	Mesh measurements on sibling devices	1.5

Note: The slab-and-stop model is described in detail in section 1.1

Table 1.62: Model Parameter Determination for Absolute Quantum Efficiency of Front-illuminated Flight Devices

in section 1.6.1.

Estimates of the errors in the relative quantum efficiency measurements were derived from the comparison of relative efficiency measurements made at MIT CSR to those made in Phase I (ACIS flat-field) of the XRCF calibration (see section 1.7.3.) Thus, at these energies, for the front-illuminated detectors, we take the standard deviation of the error in each spatially-averaged relative quantum efficiency measurement to be 0.6%, independent of energy. Fitting was performed by minimizing the χ^2 statistic. Best-fit gate-structure model parameters, along with other adopted model parameters, are listed in Table 1.63. In all cases the fits (which had but one degree of freedom each!) were statistically acceptable given the adopted measurement errors.

1.8.2.1 Fitting Methods: BI Device Model Parameters.

The spatially averaged quantum efficiency measurements described in section 1.7.2, together with the best fit absolute quantum efficiency model for detector S2 (w182c4) were used to infer absolute quantum efficiency as a function of energy for each BI device at 525 eV, 677 eV, 1740 eV, 2015 eV, 4509 eV, 5894 eV and 8040 eV. These inferred detection efficiencies exceed unity at three energies (525 eV, 677 eV and 2015 eV) in one or both BI detectors, by amounts ranging from 4% to 7%. Obviously, this result demonstrates the presence of significant systematic errors in our analysis of these data. As discussed above, we believe that one major error in our analysis arises because we do not now correct for the effects of source continuum; since the spectral redistribution functions for the BI and FI chips are quite different, the continuum contributes a larger proportion to the BI counting rate than to the FI counting rate. A preliminary discussion of this effect is presented in section 1.7.3. We have not yet completed a BI device response function model adequate for proper analysis of this data. For purposes of this report we have arbitrarily elected to retain the BI CCD deadlayer model published with the previous of of the ACIS Calibration report (October, 1997). Since continuum effects are expected to be smaller at higher energies (where the resemblance of BI and FI redistribution functions is much closer than at low energies), we have fit a model to the MIT CSR relative quantum efficiency data to determine the photosenstive thickness of each BI device, given this fixed deadlayer model. Both the fixed deadlayer model and best-fit depletion thicknesses for the BI devices are shown in Table 1.63. The quoted confidence interval for the depletion depth (15%) is based on an assumed relative quantum efficiency error of 5%.

	Model Parameters (μm)							
	Device-Specific Fit				Generic (from sibling devices)			
Location/ Device	Si	SiO_2	Si_3N_4	Depletion Depth	CS Si†	CS $SiO_2^\ddagger$	CS Width*	Reference Detector
I0/w203c4r	0.297	0.350	0.022	65	0.35	0.45	4.1	w190c3
I1/w193c2	0.292	0.339	0.024	65	0.35	0.45	4.1	w103c4
I2/w158c4r	0.272	0.319	0.030	65	0.35	0.45	4.1	w103c4
I3/w215c2r	0.291	0.344	0.020	65	0.35	0.45	4.1	w190c3
S0/w168c4r	0.264	0.318	0.024	64	0.35	0.45	4.1	w190c3
S1/w140c4r	0.0001*	0.023*	N/A	30	N/A	N/A	N/A	w134c4r, w103c4
S2/w182c4r	0.270	0.231	0.030	76	0.35	0.45	4.1	w103c4
S3/w134c4r	0.0001*	0.023*	N/A	40	N/A	N/A	N/A	w203c2, w103c4
S4/w457c4	0.244	0.314	0.042	72	0.35	0.45	4.1	w190c3
S5/w203c4r	0.289	0.339	0.021	72	0.35	0.45	4.1	w190c3
1-parameter 90% conf. limits for								
FI Devices:	±0.024	±0.008	±0.010	±1.7	fixed	fixed	fixed	
BI Devices:	fixed	fixed	N/A	±15%	fixed	fixed	fixed	

†: typical one-parameter 90 % confidence range from mesh experiments is $^{+0.06}_{-0.03}\,\mu m$.
‡: typical one-parameter 90 % confidence range from mesh experiments is $^{+0.17}_{-0.11}\,\mu m$.
⋆: typical one-parameter 90 % confidence range from mesh experiments is $^{+0.3}_{-0.4}\,\mu m$.
∗: Deadlayer model parameters for BI devices fixed at approximate values; see text.

Table 1.63: Adopted ACIS Flight Detector Quantum Efficiency Model Parameter Values

1.8.2.2 Results and Data Products

The best-fit model for each flight detector was used to predict quantum efficiency as a function of energy. For historical reasons, our fits of the model to the data (both for the absolute response of the reference detectors, and the relative response of flight detectors) made use of standard (Henke, 1993) mass-absorbtion coefficients. It should be noted, however, that the *predicted* flight detector efficiency curves incorporate our measurements of the absorption edge structure near the nitrogen, oxygen and silicon edges (see section 1.6.4).

As an example, the best-fit quantum efficiency for ACIS detector S2 (the most efficient ACIS FI detector at all energies) is shown in Figure 1.91. The lower panel of the figure shows estimated 90% confidence envelope on the relative error in the model quantum efficiency; these error limits are discussed in detail in the next section.

The adopted quantum efficiency models for the two BI devices are shown in Figures 1.93 and 1.94.

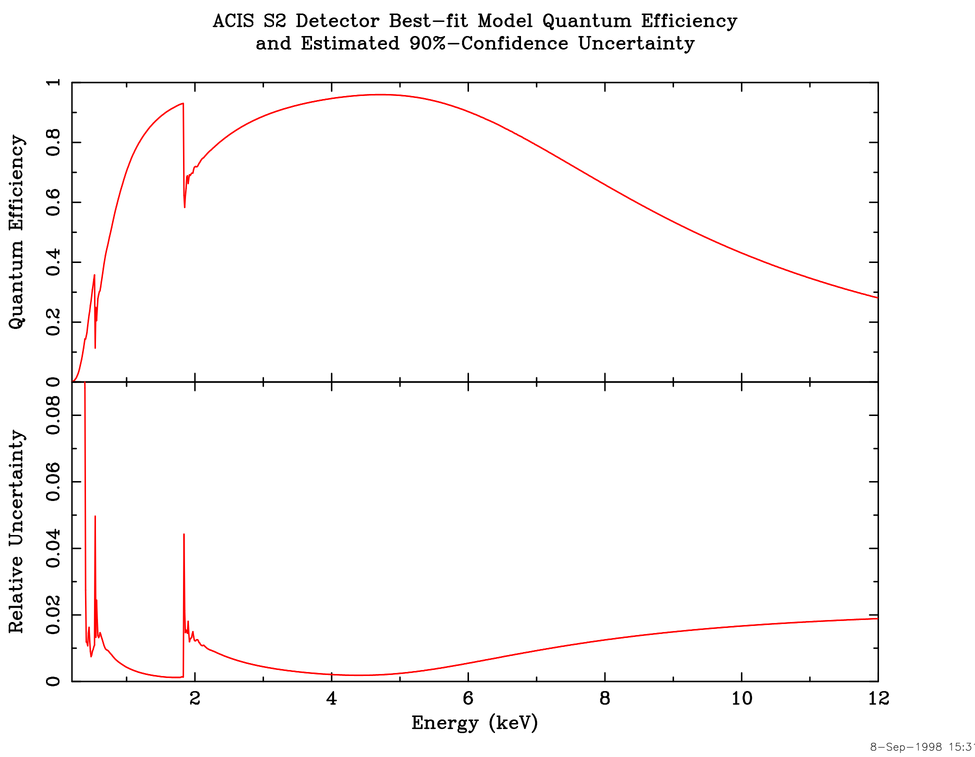

Figure 1.91: Best-estimates for ACIS S2 (Front-illuminated) Detector Quantum Efficiency Model and 90% Confidence Envelope. See text for interpretation of the error envelope.

The best-fit quantum efficiency models for all FI detectors are shown in Figure 1.92.

The quantum efficiency of the back-illuminated detector S3 is shown in Figure 1.94

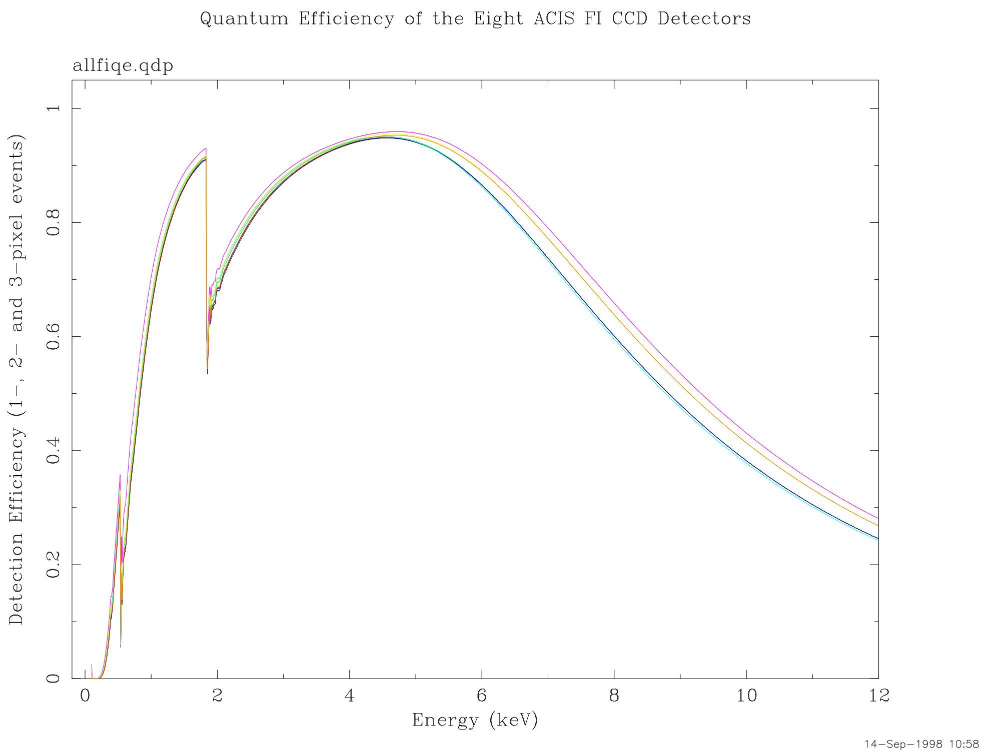

Figure 1.92: Best-fit model quantum efficiency for all ACIS FI Detectors

The quantum efficiency of each ACIS flight detector will be made available as an ASCII table file. It is intended that these files be available from the MIT ACIS web page at

`http://acis.mit.edu.`

The files can also be found on the MIT CSR ACIS calibration database in the directory

`/ohno/di/database/rsp/release.`

1.8.3 Uncertainties in Absolute Quantum Efficiency

In this section we attempt to enumerate error sources and, to the extent possible, to quantify the errors in the best-fit model quantum efficiency. It is useful to distinguish at the outset errors arising from the limited precision with which the parameters of the adopted model are constrained by the available data, on the one hand, from those arising from inadequacies

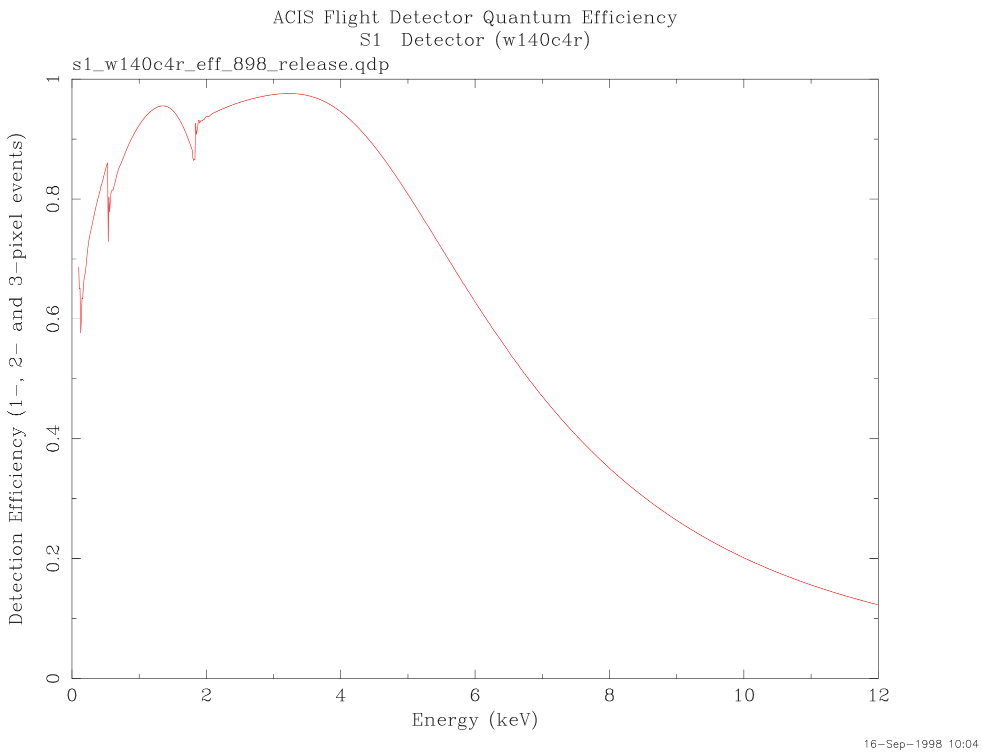

Figure 1.93: Adopted ACIS S1 (Back-illuminated) Detector Quantum Efficiency Model

in the quantum efficiency model, on the other hand. At the risk of creating some confusion, we choose to say that the former type arise from "measurement errors" since their ultimate origin is the uncertainty in the measured quantities used to constrain the model. Thus we shall sometimes use the phrase "measurement errors" as an abbreviation for "errors in predicted quantum efficiency resulting from errors in measurement." We label the latter error type "modelling errors," intending an analogous ellipsis.

In general, effects of modelling errors are difficult to quantify, and, in any event, not particularly well-bounded at this writing. In contrast, the effects of measurement errors can be quantified using well-known techniques, though it must be emphasized that even these errors must be interpreted carefully. In particular, measurement errors produce quantum efficiency errors which are NOT statistically independent from energy to energy. For many purposes it is therefore much more useful to conceive of the quantum efficiency vs. energy function itself, rather than the quantum efficiency at any particular energy, to be the random variable whose value is constrained by the model fitting.

In this section we first present a straightforward (though incomplete) quantitative anal-

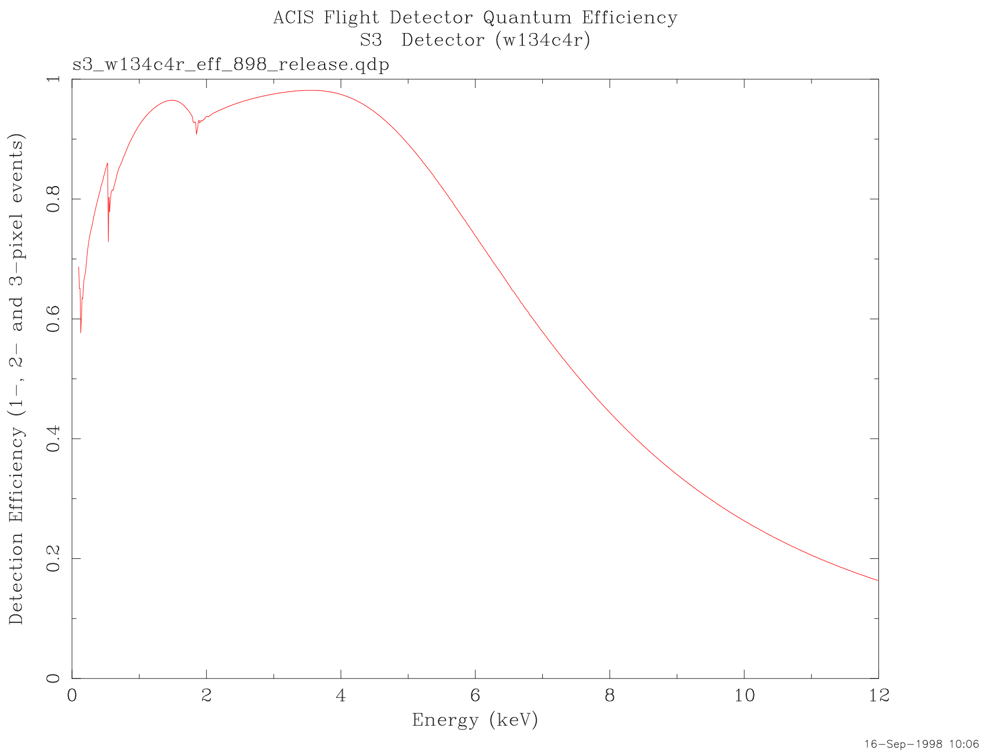

Figure 1.94: Adopted ACIS S3 (Back-illuminated) Detector Quantum Efficiency Model

ysis of the effects of measurement errors. We then discuss modelling errors. While an effort has been made to quantify modelling errors, more work remains to be done on this problem. As a result, our discussion serves mainly to guide future work.

1.8.3.1 Quantum Efficiency Uncertainties Due to Measurement Errors

To determine the accuracy of our model fits, given that the model is correct, we must define the volume of model parameter space within which model parameter values are consistent, at some level of confidence (we will adopt the 90% confidence level here,) with the data. This parameter space volume is bounded by a surface S_{90}, which we shall call the "90% confidence surface". To each point p on the confidence surface S_{90}, the model assigns a quantum efficiency vs. energy function $f_p(E)$. The ensemble of such functions $\{f_p(E) : p \in S_{90}\}$ is then the set of quantum efficiency functions just allowed, at 90% confidence, by the calibration data. A complete characterization of the quantum efficiency error would include a probability distribution of the allowed values of $f_p(E)$ for all p in the parameter space volume bounded by S_{90}. We do not provide such a characterization here.

Instead, we attempt in the following way to estimate the envelope of the functions $f_p(E)$ allowed by the data.

First, we characterize the 90% confidence surface. This surface S_{90} is defined by the property that for any point p on S_{90}, $\chi^2(p) - \chi^2_{min} = \Delta\chi^2_{crit}$, where $\chi^2(p)$ is the value of χ^2 computed for the model $f(p)$ with respect to the data, χ^2_{min} pertains to the best fit model, and $\Delta\chi^2_{crit}$ is a constant depending on the number of model parameters constrained by the fit.

In chosing $\Delta\chi^2_{crit}$, we note that the four fitted parameters belong to two distinct sets. The three gate structure parameters are entirely constrained by the low-energy ($E < 3$ keV) data, while the depletion depth is entirely determined by the high-energy data ($E = 5.9$ keV, in our case). For purposes of bounding the quantum efficiency errors, we can therefore consider the gate structure parameters separately from the depletion depth.

For three interesting parameters (the thicknesses of Si, SiO_2 and $Si3N_4$) at the 90% confidence level, $\Delta\chi^2_{crit} = 6.2$, the 90% confidence limit for a χ^2 distribution with 3 degrees of freedom. We have found the six points on S_{90} which represent the maximum deviations (both positive and negative) of each of the three gate structure parameters from their best-fit values. These are listed in Table 1.64.

Si	SiO_2	Si_3N_4	Remarks
	(μm)		
0.235	0.233	0.045	Minimum Si
0.306	0.229	0.016	Maximum Si
0.276	0.220	0.032	Minimum SiO_2
0.264	0.243	0.029	Maximum SiO_2
0.304	0.233	0.015	Minimum Si_3N_4
0.237	0.230	0.045	Maximum Si_3N_4

Table 1.64: Six points on the 90% confidence surface used to determine the uncertainty envelope for FI detector quantum efficiency.

We have evaluated the quantum efficiency model at each of these six points, and then found the extreme values of predicted quantum efficiency (among these six models) at each energy. To determine the envelope at high energy, we have separately varied the depeletion depth through its (single-parameter) 90% confidence interval of $\pm 1.7\mu m$. (Thus we have in fact sampled twelve points in parameter space, *viz.,* the six points listed in table 1.64 at the two extreme values of depletion depth. This error envelope, expressed as a fraction of the best fit model quantum efficiency is plotted as a function of energy for the S2 detector in the lower panel of figure 1.91. The plot shows the absolute value of the 90% confidence limits; positive and negative limits have been calculated, but are nearly identical, and so only the positive limits are shown.

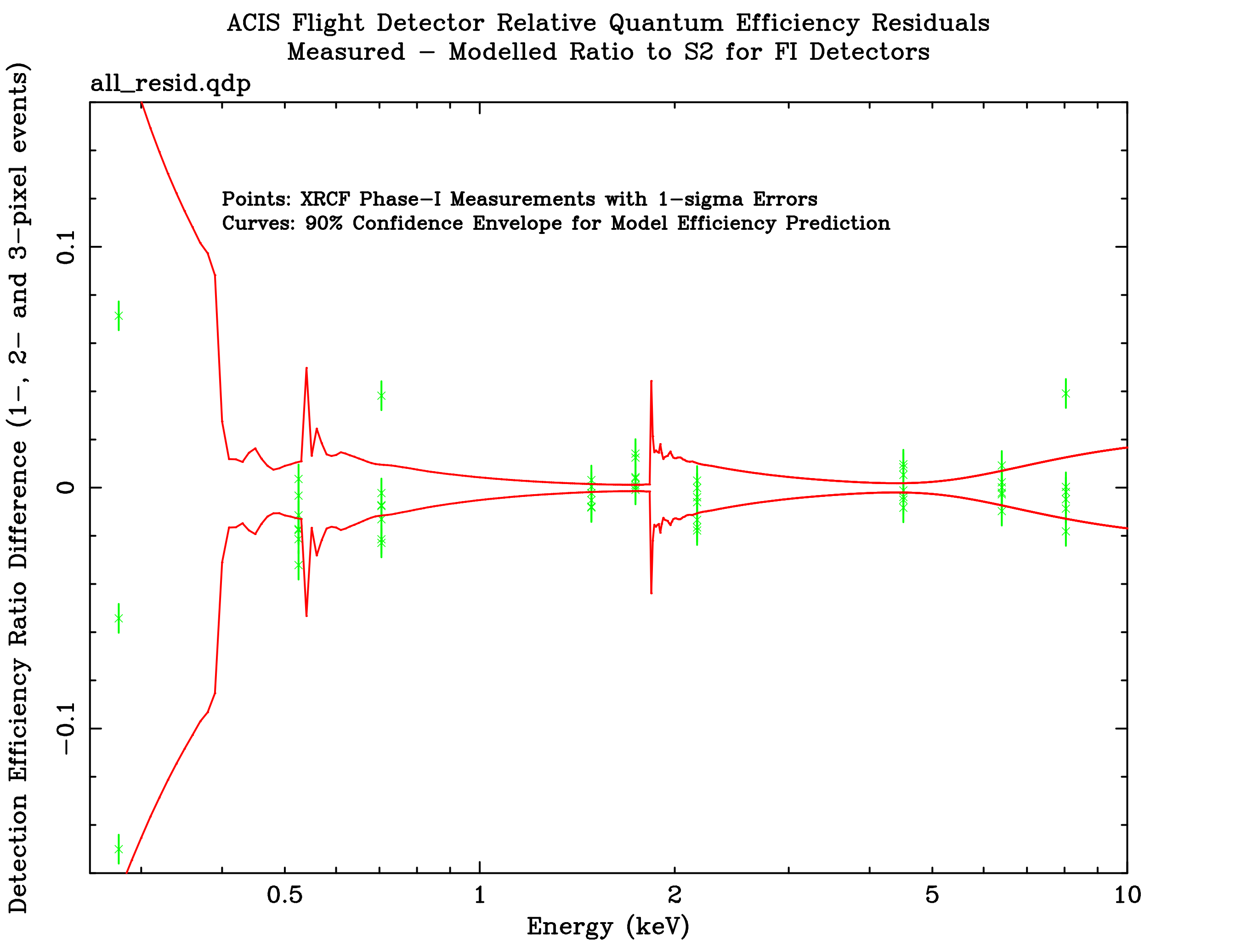

Figure 1.95: Comparison of XRCF Phase I relative quantum efficiency measurements to Model Predictions for front-illuminated detectors. Points are deviations between XRCF quantum efficiency measurements, relative to S2, and lines are estimated 90% confidence intervals for model predictions. Note that the models are based entirely on relative QE measurements made at MIT; the points shown were NOT used to constrain the models. The RMS of the residuals for energies $\geq$ 525 eV is 1.3%.

Two limitations of this error analysis must be made clear. First, we have only considered errors resulting from measurement of the flight device quantum efficiency relative to that of the reference detectors. In principle, precisely the same analysis can be performed for the absolute calibration of the reference detectors. In so doing we find that the parameter ranges allowed by fits to the reference detector response to undispersed synchrotron radiation are smaller than those shown in Table 1.64 by factors of three to six. Thus the measurement errors associated with the absolute calibration are in any case small. Moreover, since model parameter errors in the absolute and relative calibrations are presumably statistically independent, their effect on the error envelope is properly accounted for by adding a small term in quadrature to the envelope derived from the relative data alone. We have therefore chosen to ignore the effect of absolute measurement errors in the present analysis, and estimate that the resulting error in our error envelope is less than 10% of the error envelope.

A much more significant limitation of this error analysis is that we have only included effects of measurement errors on four of the seven model parameters. The three channel stop parameters have not been varied in either the absolute reference detector or relative flight detector measurements. While we have some understanding of the allowed confidence intervals for these parameters (see reference [27]), they are not constrained by measurements on the flight detectors. In principle a joint fit of the flight detector quantum efficiency data and sibling detector mesh experiment data could produce a statistically correct error estimate. We have not yet attempted to perform such a fit.

Neglect of uncertainties in the channel stop parameters may be a significant shortcoming in our error analysis. For example, we find that a 10% increase in the fixed value of each of the three channel stop parameters (the single-parameter 90% confidence limit allowed by the mesh experiments is about 10-15% in each parameter) produces a 0.5% change in the best-fit apparent synchrotron radiation intensity determined by a reference detector, averaged over the 0.4 to 4 keV band. This is comparable to the (spectrally averaged) quantum efficiency error plotted in Figure 1.91.

We believe that a mesh measurement of one of our absolutely calibrated reference detectors would provide us with quantitative information on the effects of channel stop uncertainties on the final model quantum efficiency errors.

As an independent check on these errors (and on the models!), we have compared XRCF measurements of quantum efficiency, relative to detector S2, to the ratio of model predictions for the appropriate detectors. Results are shown for seven FI devices in Figure 1.95. Also shown are the 90% confidence limits for a single model efficiency prediction. (The solid curve is NOT a predicted error envelope for the ratio of two model efficiencies.) The observed residuals are in good qualitative agreement with the quoted error limits, especially considering that the model is based entirely on fits to the MIT CSR data, while the data points come entirely from measurements at XRCF. It is clear that inclusion of XRCF data in model fits is appropriate, and would improve the accuracy of the models further, especially at energies below 0.4 keV.

Quantitative comparison suggests that the observed residuals exceed those expected from the model uncertainties and measurement errors alone, however. Excluding the three measurements at 277 eV, for which the estimated model errors are quite high (and for which the observed residuals are well within expected model errors), the mean residual for 54 measurements shown in figure 1.95 is -0.003, and the RMS deviation about that mean is 0.013. The root mean square residual (about zero, rather the mean) is also 0.013. Ignoring the correlation of model errors at different energies, and assuming that the model errors for different devices are independent, we expect the RMS deviation for the residuals, (accounting for the 0.006 1-sigma measurement errors) to be 0.0095. Thus the observed residuals are larger, by a factor 1.3, than those estimated from the model errors alone.

Several factors may account for this discrepancy. Since most of the variance in the observed residuals comes from 2 of the 54 points, (the S4 point at 705 eV and the S5 point at 8040 eV), it seems likely that some unknown systematic errors (at the 3-4% level) affect these points. With these fairly obvious outliers excluded, the residuals (at 0.009, RMS) are consistent with the model error estimates. In addition, one might expect the internal correlation of errors within any one model to increase the observed variance of the residuals. On the other hand, the model error envelopes do not account for uncertainties in the channel stop parameters, and so must be underestimates at some level.

In any event, we conclude that the our models predict relative quantum efficiency of the ACIS FI detectors with an accuracy better than 1.5%, RMS, over the 0.4 to 8 keV band. Our estimates of the errors in the models are reasonable agreeement with the data, though the errors might be understimated by 30% or so.

1.8.3.2 Quantum Efficiency Uncertainties Due to Modelling Errors

In this section we discuss modelling errors, as defined above, and their effects on both the absolute calibration of reference detectors and the relative calibration of flight detectors with respect to those reference detectors.

1.8.3.2.1 Sources of Modelling Errors in the Absolute Calibration of Reference Detectors. The CCD response model used to analyze the undispersed synchrotron radiation data suffers from a number of shortcomings. The magnitidue of the quantum efficiency errors resulting from these limitations is not well known at present. In principle, simulations comparing the accuracy of the simple models we have used to more realistic (and complicated) models could provide estimates of the magnitude of these errors. Indeed, we have already implemented more elaborate CCD models in our simulations (see section 1.14). The best approach, however, would be to fit these more sophisticated models to the calibration data. There is no technical reason why this could not be done in the near future.

For purposes of guiding such work, we list the major shortcomings of the model we used to establish the absolute response of ACIS reference detectors.

1. *The gate structure model is oversimplified.* The slab and stop model ignores gate overlaps and phase-to-phase variations in gate thickness. The resulting error varies in lowest order as the square of the optical depth of the gate structure, so in the limit that the gates are optically thin, the error vanishes. Conversely, the magnitude of this error is largest just above the absorption edges of oxygen and silicon, and at very low energies. This error can readily be quantified via simulation.

2. *Absorption fine-structure was ignored in determing model parameters.* The undispersed synchrotron radiation data were analyzed using standard Henke (1993) absorption coefficients; these omit edge structure which we have since measured (see section 1.6.4.) While the spectral resolution of the detector tends to smooth the fine structure, we have not yet established the magnitude of error introduced by neglect of fine structure. The relatively large residuals from the best-fit model (see section 1.6.1) near the absorption edges probably reflect this error. We hope to repeat the reference detector fits with the fine-structure included in the near future.

3. *The redistribution function is oversimplified.* A phenomenological representation of the spectral redistribution function has been used in analysis of synchrotron radiation data. The response to a monochromatic input is modelled as the sum of 2 Gaussians plus a phenomenological low-energy tail. A better, physically-grounded model of the redistribution function is now available (see sections 1.3.2 and 1.14), but has not yet been used to analyze the PTB/BESSY data.

   A more subtle but related difficulty is that aside from the fact that in our current model the channel stop is taken to be a dead volume, there is no allowance for variation of the redistribution function with position within a pixel. A more realistic picture is that the spectral redistribution function for photons absorbed in the channel stops is non-zero but differs markedly from that for the rest of the device. We are now modelling this effect.

4. *Channel stop parameter values have not been measured directly for the reference detectors.* The most reliable measurements of channel stop dimensions are obtained using the mesh technique described in section 1.5, and from (destructive) scanning electron micrographs. Neither of these techniques has been applied to determine the

channel stop parameters of the reference detectors themselves. It is hoped that mesh measurements can be made on at least one of the reference detectors.

5. *Spatial variations in quantum efficiency have not been physically modelled.* While the method used to infer depletion depth is simple and apparently reasonbly accurate, it is subject to a number of systematic errors, as has been discussed in section 1.6.2. Of particular note are variations in depletion depth with position in each detector. The branching ratio data show small (several microns out of 65-75 microns) variations in depletion depth from quadrant to quadrant within a detector. Thus the use of spatially averaged quantum efficiency may lead to systematic errors at high energy. Indeed the quantum efficiency maps (see section 1.7) show some modest ($\sim 2-3$) residual variation with detector position at 8 keV; little, if any, such variation is seen at lower energies in the FI devices. While we believe the best interpretation of these variations is that they reflect spatial variation in the depletion depth, this interpretation is speculative.

1.8.3.2.2 Magnitudes of Modelling Errors in the Absolute Calibration of Reference Detectors We have identified several lines of evidence that can supply quantitative bounds on systematic measurement errors, and on some kinds of modelling errors. Taken together, these checks furnish some confidence that, for front-illuminated devices, the absolute quantum efficiency errors are no larger than 5% in the 0.4 - 4 keV band.

1. *Plausibility of best-fit model parameters.* The best-fit values for synchrotron radiation flux normalizations, relative to the expected value, for three reference detectors discussed in section 1.6.1 are 1.000,0.994, and 0.956, respectively; these numbers each have 90% confidence intervals of approximately ± 0.005. The simplest interpretation of these results is that any residual systematic errors in the broad-band quantum efficiency amount to less than 5%. Moreover, the inferred mean gate structure parameters are in the range (within $\pm 50\%$) expected given the device fabrication process, suggesting that the slab and stop model is providing a reasonable, and therefore probably reliable, representation of the gate structure.

2. *Internal consistency of reference detector quantum efficiencies.* The quantum efficiency models derived for the reference detectors from synchrotron radiation data can be compared to relative efficiency measurements made at MIT CSR. The ratio of the two models agrees quite well with the relative quantum efficiency data: for the five energies measured at MIT within the BESSY passband (0.525 to 4.5 keV), the residuals (measured ratio minus modelled ratio) have a mean of -0.008 and a standard deviation of 0.01. Thus the mean is consistent with 0 at the 2-sigma level, provided

the standard deviation is taken to be measure of the random errors in the residuals. The latter assumption is a good one, given that the errors in the relative quantum efficiency measurements are thought to have a standard deviation of 0.6%.

This result suggests that, although it cannot be ruled out at present, it is unlikely that broadband errors as large as 5% could remain in the absolute quantum efficiency models of the reference detectors, at least in the BESSY passband.

Of course our internal consistency check cannot rule out all systematic errors. For example, this check would not reveal a geometry error that affected every BESSY measurement identically (though the normalization results described above suggest such an error is highly unlikely.) It is noteworthy, however, that the synchrotron measurements in question were made on different runs separated in time by about a year, and with different sets of electronics.

3. *Comparison to other absolutely calibrated detectors* An extremely valuable check on ACIS absolute efficiency models will be provided by comparisons to absolutely calibrated beam normalization detectors at XRCF. The most suitable detector for this purpose, the solid-state detector (SSD), has been calibrated at the same PTB beamline that was used to calibrate the ACIS reference detectors. As of this writing, the absolute response of the SSD is not yet available, however, so this important check remains to be done.

   Nevertheless, since the SSD detector is thought to be fairly well understood at higher energies, and since we have no other external check on our high-energy absolute calibration, we have compared the ACIS flight detector model predictions to ACIS-to-SSD relative QE measurements made at XRCF. The XRCF phase-I results used for this purpose are detailed in table 1.36 in section 1.6.6. If we use the ACIS detector model quantum efficiencies, together with these relative QE data, to infer the detection efficiency of SSD5 at 8.040 keV, we obtain ten estimates of the SSD5 efficiency. The mean value of these estimates is 0.966, and the standard deviation of the estimates is 0.033. For the FI detectors alone (for which the QE model is based on the branching ratio technique), the mean is 0.952, and the standard deviation os 0.018. The a priori expected quantum efficiency of the SSD5 at this energy is 0.997 (according to R. Edgar). This comparison is thus consistent with the supposition that systematic errors in the absolute efficiency of our models for the FI detectors are no more than 5%.

   We emphasize that a more precise characterization of ACIS systematic errors, especially at energies above 4 keV, awaits absolute calibration of the XRCF BNDs to an accuracy of order 5% or better. The calibration of SSD5 would be the most useful for this purpose.

1.8.3.2.3 Sources of Modelling Error in the Calibration of Flight Detectors Relative to Reference Detectors. Generally, the relative quantum efficiency measurements are subject to fewer errors, of smaller magnitude than those afflicting the absolute measurements. Nevertheless, the model used to interpret the relative quantum efficiency contains a number of implicit assumptions which are not directly verified by the calibration measurements. Following is a list of some potential "modelling errors" that could affect the accuracy of the relative quantum efficiency model. Future work could, in principle, quantify some of these errors more precisely.

1. *Differences between spectral redistribution functions of flight and reference detectors.* Our model of the relative quantum efficiency measurements implies that differences in efficiency are due to differences in gate structure thickness or depletion depth. Thus we make no correction for differences in the branching ratios or tail amplitudes of the spectral redistribution function (though differences in the spectral resolution are accounted for). For FI-to-FI device relative measurements, the effects of any such differences are minimized because i) we have chosen an event grade set which is known to be substantially independent of energy in the 0.5 - 2.1 keV band, for any given CCD and ii) the sources used are quasi-monochromatic.

   On the other hand, quantum efficiency measurements of back-illuminated flight devices relative to the (front-illuminated) reference detectors are much more sensitive to errors from this source, since the redistribution function is so different for the two types of detector. Indeed, this difference, coupled with the spectral complexity of the X-ray sources used, is believed to cause significant systematic errors in our current analysis of the relative quantum efficiency data.

   At present we have no direct estimate of the size of errors introduced by differences in spectral redistribution functions in FI-to-FI relative efficiency measurements. The consistency of relative quantum efficiency measurements made at MIT and XRCF implies that such errors are not large, at least for the front-illuminated devices. See below.

   Errors in BI-to-FI device efficiency arising from this source are discussed in some detail in section 1.7.3. Depending on the source spectrum, such errors can range in size from 5% to 25%.

2. *Spectral complexity in the source.* The current interpretation of relative detection efficiency measurements presumes that the source is monochromatic. In fact, none of the sources used is monochromatic. As discussed above, the error introduced by

complexities in the source spectrum is coupled to differences in the response functions of the flight and reference detectors. This error is certainly more important for measurements of back-illuminated flight detectors relative to front-illuminated reference detectors.

One bound on the magnitude of such errors is provided by a comparison of relative quantum efficiency measurements made at XRCF to those made at MIT CSR, since the "out of band" spectra of the sources at the two sites was generally quite different. In general, the agreement for FI-to-FI detector comparisions is quite good (1.1% RMS below 8 keV), while BI-to-FI detector relative efficiencies are not so reproducible.

3. *Differences in channel stop parameters in the the flight and reference detectors.* The most reliable measurements of channel stop dimensions are obtained using the mesh technique described in section 1.5, and from (destructive) scanning electron micrographs. Neither of these techniques has been applied to determine the channel stop parameters of the flight or reference detectors themselves. Since differences in channel stop parameters are not included in the relative quantum efficiency model, any such differences would be modelled incorrectly. In principle, measurement of channel-stop parameters on a number of siblings of the flight devices (via mesh experiments) could bound the size of errors due to channel stop variations.